Proc. Estonian Acad. Sci. Engng., 1999, **5**, 1, 22–40
https://doi.org/10.3176/eng.1999.1.02

LINEAR ROSSBY WAVES AND ZONAL TRANSPORT IN ROTATING PLATFORM

Tarmo SOOMERE[a] and Tiit KOPPEL[b]

[a] Estonian Marine Institute, Paldiski mnt. 1, 10137 Tallinn, Estonia
[b] Tallinn Technical University, Ehitajate tee 5, 19086 Tallinn, Estonia

Received 13 March 1998, in revised form 1 October 1998

Abstract. Rossby waves and their interactions were studied experimentally in the "Coriolis" rotating tank. The geographical β-effect was modelled by a planar sloping bottom. Travelling waves with typical velocities of fluid particles about 1 mm/s were excited by a small radially oscillating paddle. In many experiments, a noticeable zonal transport in the form of weak jets, with a typical width of 0.4–1.0 m and velocity about 0.4 mm/s, was detected after about 10 wave periods. In some cases, it lead to water displacements by a distance comparable to the paddle amplitude. The transport was most probably induced by wave-wave interactions within a stochastic wave field which arose due to reflections of waves as well as to non-homogeneities of the bottom and the walls.

Key words: Rossby waves, weak nonlinearity, zonal flow.

1. INTRODUCTION

1.1. Linear Rossby waves, nonlinear synoptic vortices and zonal flow

The Rossby wave is an example of transversal low frequency oscillations found in rotating systems. It owes its existence to the variation of the vertical component of the background rotation (in geophysics – the north-south variation of the Coriolis parameter, called β-effect). Rossby (planetary) waves (defined as linear disturbances propagating in a medium) and synoptic vortices (cyclones and anticyclones in the atmosphere, synoptic rings in the oceans – nonlinear structures carrying medium with them) are the main examples of synoptic(-scale) motions. They both can be described by the quasigeostrophic vorticity equation and the border between them often depends on the taste of the investigator.

Synoptic motions in nature are usually their mixture: superposition of linear Rossby waves typically resembles a system of vortices, and a single synoptic vortex generally radiates waves [1]. This feature (although it enables explanation of the recordings of synoptic vortices in terms of superposition of wave harmonics [2,3]) complicates understanding of these processes since one cannot determine the level of nonlinearity from a single snapshot of the motion.

A remarkable property of synoptic motions (also called geostrophic turbulence) is energy transfer to larger scales. The process is accompanied by supporting an anisotropic flow, directed along parallels, and called zonal flow. Both features are usually thought to characterize the nonlinear flow. However, after a long time geostrophic turbulence must become spectrally isotropic [4] and the zonal flow should vanish. In nature, this is not the case: in the atmosphere, the overwhelming domination of the zonal wind component is well known and the ocean currents mostly flow in the east-west direction. Also, apart from jet-like currents the zonal component of ocean motions frequently dominates [5].

The anisotropization might be, at least, partially created by Rossby wave interactions since they always support zonal flow. Theoretically, systems of barotropic Rossby waves evolve towards a special equilibrated state, consisting of a superposition of the zonal flow and the spectrally isotropic wave system [6–10]. This feature probably holds for arbitrary vertical structure of the medium [11–13]. According to estimates [14], nonlinear vortices cover only about 20% of the ocean area. Thus, one can even hypothesize that synoptic vortices exchange energy through Rossby waves, interaction of which leads to zonal flow amplification.

1.2. Experimental studies of Rossby waves

Rossby waves have been studied experimentally over 30 years, mostly in the framework of laboratory modelling of the ocean circulation. Although the latter go back as far as to the experiment performed by Bjerknes at 1902 [15], Rossby waves were probably first detected in early experiments by Fultz, Frenzen, and Kaylor [16,17]. Phillips [18] proposed a simple device for their modelling, showing that low-frequency waves in a rotating annulus with a parabolic bottom are identical to Rossby waves in a β-plane channel. Ibbetson and Phillips [19] performed classical experiments with this device and a paddle wavemaker. Pedlosky and Greenspan [20] introduced another model, a rotating annulus with a linear sloping bottom, to demonstrate how the general theory for homogeneous rotating flows must be modified for a basin with not closed depth isolines. Holton [21] used this model first. Beardsley and Robbins [22,23] used a rapidly rotating cylinder with a planar sloping bottom (called sliced-cylinder model). A thorough study of (quasi)geostrophic flows was performed by Colin de Verdière [24] who, like Holton [21], used the source-sink method for forcing the flow. He

verified that eddies can feed zonal flow with energy. Like Whitehead [25], he also mentioned the possibility to transfer energy from Rossby waves to mean flow. However, this effect was not fully separated from turbulent forcing and Stokes drift, usually associated with the large paddle amplitudes in this and some other experiments [26]. Detailed investigations into dynamics of synoptic eddies are described by Nezlin [27].

However, until now the investigators have difficulties in exciting long-living Rossby waves and isolating a travelling wave from eddies and mean flow. Modelling alterating background rotation is complicated in itself. With the source-sink method one may excite a limited set of waves. Paddle wavemaker requires special measures in order to prevent flow around its edges [19]. Typically, owing to large viscous and Ekman damping (caused by large wave amplitudes), only one or two wave crests nearest to the paddle are detectable. As a result, the earlier experiments considered a limited set of large-amplitude Rossby waves. Observations were mostly made in the near-wave field, from which one can establish main features of waves but cannot capture fine details of the wave evolution.

In this study, an attempt is made to isolate Rossby-wave dynamics from geophysical turbulence through keeping the wave amplitudes as small as possible. This approach ensures applicability of the approximations made in deriving the quasigeostrophic vorticity equation for slow motions in the rotating tank (frequently poorly satisfied in earlier experiments). To take a look at the nonlinear energy exchange between wave harmonics, evolution of practically linear waves during a great number of wave periods has been tracked. Small-scale nonhomogeneities of the bottom and the walls were thought to redistribute the initial wave energy in a long-time run to a spectrally broad wave system. According to the kinetic theory, the latter should give rise to low-frequency wave harmonics propagating along the tank radius. The main goal of the experiment was to detect these harmonics in the form of striped flow along bottom isolines (equivalent to zonal flow).

In this paper, mostly qualitative results of the wave experiments will be described. The nontraditional experimental setup and the novel correlation image velocimetry (CIV) method [28] will be described in some detail. Since the equation for Rossby waves on a β-plane is identical to that of drift waves in plasma, the results might be of interest in plasma physics.

2. EXPERIMENTAL SETUP AND GOVERNING EQUATIONS

2.1. Modelling the β-effect. Zonal channel and mixed geometry

Experiments were performed in the "Coriolis" Laboratory of Geophysical Flows, Joseph Fourier Grenoble University, on the rotating platform with the

diameter 13 m. The rotation period of the tank was mostly 50 s; the water depth was 50 cm with no stratification and the rotation direction – counter-clockwise.

For the intent of the study, the sliced-cylinder model (excluding any mean flow) was not apt and a version of radially symmetric bottom topography for simulating the geographical β-effect was used. Erection of a paraboloidal bottom would have been too expensive and not suitable for accompanying experiments. A sloping bottom in the general form of a curved trapezoid with its outer length of about 16 m and width of 4 m (covering about 52 m^2, i.e. 40% of the platform perimeter) was built from plain segments of 2×2 m (Fig. 1). The 8%-slope begins at the distance of 2.5 m from the rotation centre and raises the outer edge of the tank. In

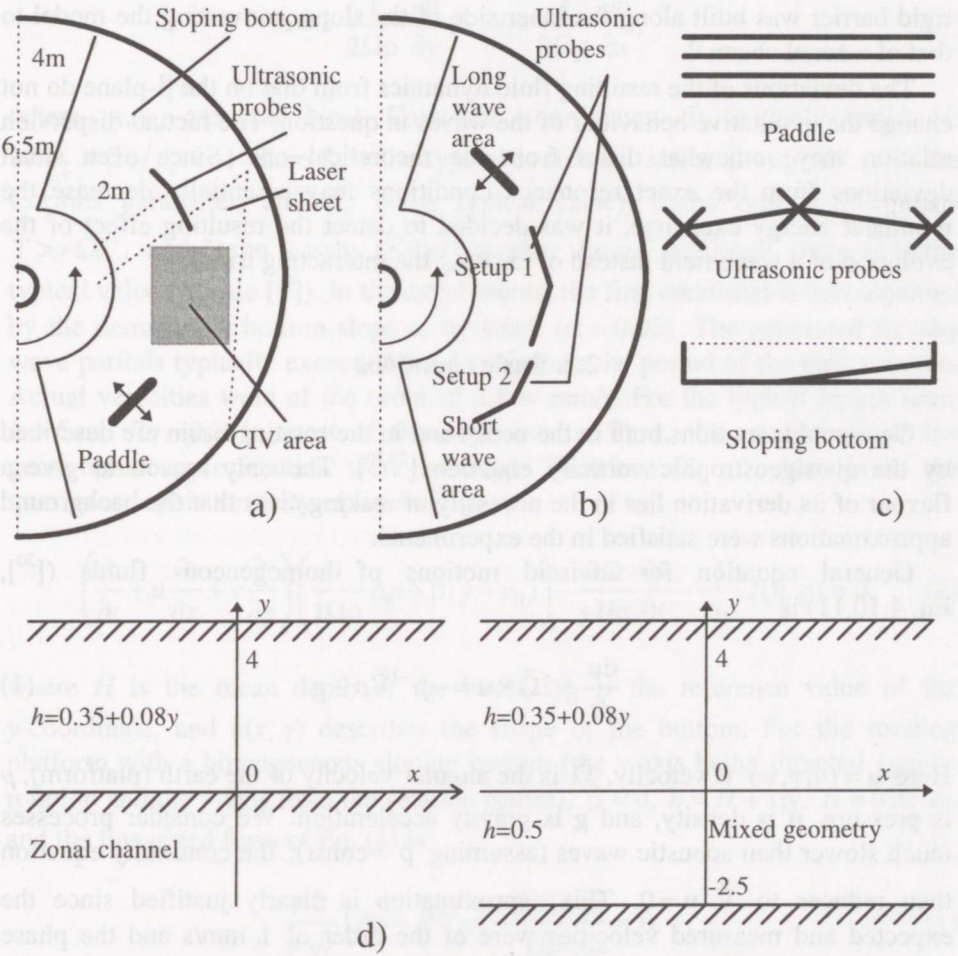

Fig. 1. a) The basic configuration of the experiments with the CIV method; b) setups 1 and 2 of the paddle and ultrasonic sensors; c) scheme of the paddle, contact measurement points and the sloping bottom; d) models of the zonal channel and mixed geometry.

this geometry, direction to the north is from the rotation centre to the outer edge; wave crests propagate in the direction of rotation (westwards); shorter waves arise eastwards from the wavemaker and the longer ones – westwards from it.

The advantage of this "intermediate" configuration is its simplicity, and it locally represents the topographical β-plane. Another argument for this setup comes from the implicit interest in the spectrally broad wave field. The bottom inhomogeneities (junctions of the segments) were supposed to serve as weak sources of random waves. The open boundaries of the slope (except the rigid outer edge of the tank) absorbed the wave energy and prevented both the growth of standing waves and the meridional wavenumber selection connected with the finite size of the device. This pattern (called mixed geometry) models, e.g., topographic Rossby waves on a continental slope. For a part of experiments, a rigid barrier was built along the inner side of the slope, converting the model to that of a zonal channel.

The deviations of the resulting fluid dynamics from that on the β-plane do not change the qualitative behaviour of the waves in question. The factual dispersion relation may somewhat differ from the theoretical one. Since even small deviations from the exact resonance conditions may essentially decrease the nonlinear energy exchange, it was decided to detect the resulting effect of the evolution of a wave field instead of exciting the interacting triads.

2.2. Basic equations

Geostrophic motions both in the ocean and in the rotating basin are described by the quasigeostrophic vorticity equation [29,30]. The only reason to give a flavour of its derivation lies in the necessity of making clear that the background approximations were satisfied in the experiments.

General equation for inviscid motions of homogeneous fluids ([30], Eq. 4.10.11) is

$$\frac{\mathrm{d}\mathbf{u}}{\mathrm{d}t} + 2\vec{\Omega}\times\mathbf{u} = -\rho^{-1}\vec{\nabla}p - \mathbf{g}\,. \qquad (1)$$

Here $\mathbf{u} = (u, v, w)$ is velocity, $\vec{\Omega}$ is the angular velocity of the earth (platform), p is pressure, ρ is density, and $\mathbf{g}$ is gravity acceleration. We consider processes much slower than acoustic waves (assuming $\rho = \mathrm{const}$); the continuity equation then reduces to $\vec{\nabla}\cdot\mathbf{u} = 0$. This approximation is clearly justified since the expected and measured velocities were of the order of 1 mm/s and the phase velocities of the Rossby waves – of the order of a few dozens cm/s. Also, the vertical displacements are negligible as compared to the reduced depth of the basin.

Since the background rotation suppresses the vertical velocity component, use of the hydrostatic approximation ([30], Eq. 5.6.1)

$$\frac{dp}{dz} = -\rho g, \tag{2}$$

is justified. It makes possible to eliminate the vertical velocity component from Eq. (1). The vertical velocity was not measured (it was much below the resolution of the measurement techniques), but we were repeatedly impressed by the beauty of two-dimensionality of the motions.

The geostrophic approximation reads:

$$u = -\frac{1}{2\Omega\rho}\frac{\partial p}{\partial y}, \quad v = \frac{1}{2\Omega\rho}\frac{\partial p}{\partial x}, \tag{3}$$

where x, y are the local Cartesian coordinates. It is only valid if: 1) $\varepsilon_L = \beta L / f_0 << 1$ (here L is the typical horizontal scale, $\beta = df/dy$, f is the Coriolis parameter, and f_0 is its typical value), 2) the typical time scale $T >> \Omega^{-1}$, and 3) the Rossby (Kibel) number $Ro = U/(fL) << 1$ (here U is the typical velocity scale [30]). In the experiments, the first condition is accompanied by the demand for bottom slope to be small ($\alpha = 0.08$). The generated Rossby wave periods typically exceeded for 4 to 6 times the period of the tank rotation. Actual velocities were of the order of a few mm/s. For the typical length scale $L = 5$ m, $Ro \approx 0.1$ in most of the experiments. Thus, the restrictions of the geostrophic approximation were satisfied. Therefore Eq. (1) reduces to the quasigeostrophic vorticity equation [29]

$$\left(\frac{\partial}{\partial t} + u\frac{\partial}{\partial x} + v\frac{\partial}{\partial y}\right)\left(\frac{1}{1\Omega\rho}\Delta p + \beta(y - y_0)\right) - \frac{2\Omega}{gH\rho}\frac{\partial p}{\partial t} - \frac{1}{H\rho}J(h, p) = 0, \tag{4}$$

where H is the mean depth of the basin, y_0 is the reference value of the y-coordinate, and $h(x, y)$ describes the shape of the bottom. For the rotating platform with a homogeneous sloping bottom (the x-axis being directed against rotation and the y-axis from the rotation centre), $\beta = 0$, $h = H + \alpha y$, $H = 0.35$ m, and the linearized form of Eq. (4) is

$$\frac{1}{\rho}\frac{\partial}{\partial t}\left(\Delta p - R^{-2}p\right) + \frac{2\alpha\Omega}{H\rho}\frac{\partial p}{\partial x} = 0. \tag{5}$$

The dispersion relation for Rossby waves on the infinite slope reads:

$$\omega = -\frac{2\alpha\Omega}{H}\frac{k}{k^2 + l^2 + R^{-2}}. \qquad (6)$$

Here $R = \sqrt{gh}/2\Omega$ is the barotropic Rossby radius, and $\mathbf{k} = (k,l)$ is the wave vector. Equation (6) demonstrates that formally Rossby wave periods may be of any value depending on the slope α, but from the above follows that, for small periods, approximations made in deriving Eq. (4) become invalid. The presence of boundaries leads to wavenumber selection in Eq. (6). In the case of an infinite zonal channel the meridional wavenumber k is arbitrary but the zonal one may take only the values $l_n = n\pi/A$, where $n \geq 1$ and A is the channel width. For this choice, the periods of the Rossby waves exceed at least twice the tank rotation period, a general feature of second-class oscillations [18]. For $A = 4$ m and rotation period $T = 50$ s, the Rossby waves have the minimum period $T_{\min} \approx 174$ s [31]. The case $n = 0$ corresponds to Kelvin waves for which radial displacements vanish identically. Their period is about 29 s (27 s for experiments with the tank rotation period 47–48 s). Without the inner barrier, Rossby waves extend to the area with horizontal bottom. Assuming that wave amplitudes decrease there exponentially, their dispersion relation qualitatively coincides with that for an infinite plane and zonal channel (Fig. 2). The minimum period of Rossby waves in this setup was $T_{\min} \approx 142$ s [31].

3. WAVE EXPERIMENTS

3.1. Remote and contact measurements

The CIV method [28] was first used for remote measurements of the two-dimensional (2D) Lagrangian velocity field in a large area (about 2×2.5 m). Small drops of fluorescent dye solution (instead of particles for the classical

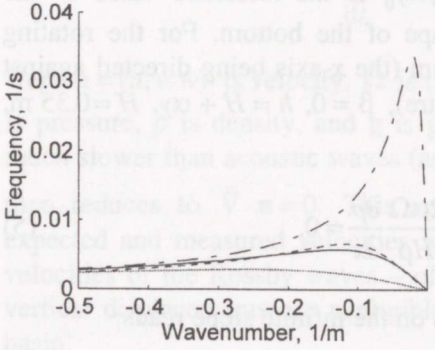

Fig. 2. Dispersion relation of Rossby waves for infinite slope ($l = 0$ – dashed-dotted line), zonal channel ($l = 1$ – continuous line, and $l = 2$ – dotted line), and mixed geometry (dashed line).

particle image velocimetry method) were randomly distributed into the water. They fast formed a practically 2D field of small-scale structures. The dye was activated by a laser beam at the depth of 12 cm. The background rotation effectively suppressed the vertical velocity and its variation over the beam thickness (5–10 mm) was negligible. The horizontal velocity components were computed on the basis of displacements of dye structures. The hardware in use (based on a digital video camera with the resolution 724×468 pixels) and the physical phenomena allowed us to obtain 2D velocity fields with an actual resolution 60×80 points. The computed velocity fields contained a few clearly incorrect values, occurring owing to the lack of dye in some regions of the measurement area, to dust particles on the water surface, to outside light flashes or to inhomogeneities of the black bottom. Erroneous values were excluded manually. We attempted to correct suspect values with the maximum likelihood techniques, restricting both the velocity and vorticity fields to be smooth.

The CIV method has relevant advantages in measuring wavy and rotating movements of water concerning the contact measurement techniques. Nevertheless, due to its modest temporal resolution, additionally two Eulerian velocity components in three points had been measured with ultrasonic MINILAB (Model SD-12) by Sensordata (Bergen, Norway) with guaranteed resolution 1 mm/s, bandwidth 35 Hz, and effective acoustic pathlength 29 mm. The actual resolution of most of the probes was much better, at least, of the order of 0.2 mm/s. The sensor pairs were mounted at a fixed distance 4.5 m from the centre of the platform (i.e., at the middle position of the paddle). Each sensor measured velocity at an angle 45° with respect to the radial direction. The distance between the pairs was 1 m. Calibration of the probes has been performed *in situ* on the basis of the recorded jerky velocity changes after the rotation speed of the tank was quickly increased or decreased.

Background motions in the basin were carefully minimized. The wind stress was neutralized through fences mounted at each 2 m on the basin perimeter about 1 m above the water. Until the end of the experiments, the average zonal velocity was less than 0.005 mm/s (Fig. 3). There was no detectable local zonal flow: flow had no directional preference and absolute value of its velocity was less than 0.1 mm/s. Measurements were delayed, at least, two hours after starting the rotation of the platform (or after filling it) until the water achieved the solid body rotation state and the rms background velocity field decreased under 0.3 mm/s.

3.2. Wave patterns and dispersion relation

The waves were excited by a robust paddle (Fig. 1c) consisting of four vertical aluminium blades of $100 \times 30 \times 1$ cm. It was mounted at the (radial) middle point of the slope and oscillated sinusoidally with a typical amplitude of

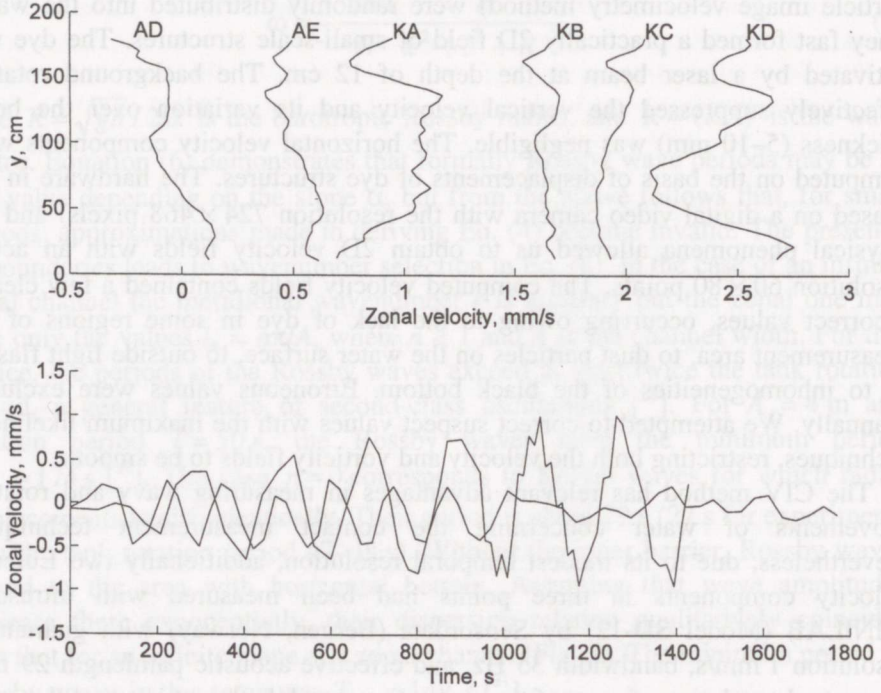

Fig. 3. Average zonal velocity of the background motions (above – averaged over the x-direction; the graphs are shifted by 0.5 mm/s with respect to each other), and during the experiments t10 and t11 (below – averaged over the whole measurement area).

35 cm. Only waves travelling along bottom isolines (i.e., with $l = 0$) were produced. Since the wavelengths greatly exceeded the extent of the paddle, it functioned in the regime of an acoustic shortcut and thus gave rise only to (resonantly excited) free waves. A list of wave experiments is given in Table 1.

In experiments with the paddle period $P < T_{\min}$ no travelling waves existed. Only the sensor closest to the paddle (Fig. 1) recorded a disturbance in the paddle period (the near-wave field). Its amplitude decreased more than of an order at the second measurement point and was indistinguishable from the background motions at the third point (Fig. 4a). A part of the wave energy was transformed into inertial oscillations with period close to a half of the tank rotation period. Also, a peak corresponding to Kelvin waves appeared in the farthest measurement point.

Starting from $P = 160$ s (mixed geometry) and $P = 200$ s (channel) the sensors recorded well-defined westward-propagating disturbances in the paddle frequency. At the short-wave side of the paddle they rapidly (within one period after the paddle signal arrived) obtained a stationary amplitude. At the long-wave side their amplitude continued to grow during 4–5 periods and remained much

Table 1. List of wave experiments[1]

Paddle period, s	Experiments with ultrasonic sensors at the down-rotation side (long-wave area): File (cycles, setup no., paddle amplitude, if not equal to 300 mm)	Experiments with ultrasonic sensors at the up-rotation side (short-wave area)	CIV: (name: no of frames)
65	a3 (15*8*200 mm)		–
80	a4 (15*8*250 mm)		–
100	a8 (15*8), b1 (10*7)	h0 (15*1zon), h6 (15*1zon*300), h9 (15*1), h15 (15*1*300)	–
130	a9 (15*8)	h1 (15*1zon), h10 (15*1), t10 (7*3)	t10(KC:63)
140		t5 (10*1), t8 (6*3)	
150		t3 (10*2), t7 (7*1)	
160	a10 (10*8), a15 (15*9), a17 (30*8), b0 (10*7), a19 (15*10), c2 (30*8), c3 (10*10), e1 (10*5), e2 (6*6), e3 (10*6)	h2 (15*1zon), h11 (15*1), h16 (15*2)	a13(A1:45), a15(AB:91), a19(AC:52), e1(AD:51), e2(AE:27), e3(AF:101)
170		t4 (10*2), t6 (7*1)	
200	a11 (10*8), a18 (25*8)	h3 (15*1zon), h7 (15*2zon), h12 (15*1), t0 (15*2), t9b(7*3), t11 (7*4)	t9b(KB:67), t11(KD:70)
250	a12 (10*8), b2(10*7), c0(25*8)	h4 (15*1zon), h8(15*2zon), h13 (15*1), t1 (15*2)	–
300	a13 (15*9), a14 (15*8)	h5(15*1zon), h14(15*2), t2(10*2), t9a(7*3)	t9a(KA:70)

[1] The tank rotation period is 47.48 s for the experiments a3–a13 and 50 s afterwards. The paddle amplitude is 35 cm except in experiments a3 (when it was 20 cm), a4 (25 cm) and a8, h6, h15 (30 cm).

Setup 1 is standard for paddle-generated waves (Fig. 1). For setup 2, the sensors are moved by 3 m in the down-rotation direction. Index "zon" at setups 1 or 2 means that the experiment was performed in the zonal channel. Setup 3 contains the CIV area in the short-wave region, the paddle being slightly replaced. Setup 4: the CIV in the long-wave area, paddle in the mirror reflection to setup 2. Setup 8 is the mirror reflection of 1 with respect to the centre of the sloping bottom. Setup 7 (experiments b0, b1, b2 only) is as 8 but without the sloping bottom. Setup 9 is obtained from 8 by replacing sensors so that the CIV area lies between them and the paddle. Setup 10: the CIV area is in the up-rotation direction from the paddle and the sensors at the border of the sloping bottom. Setups 5 and 6 were used in accompanying experiments only.

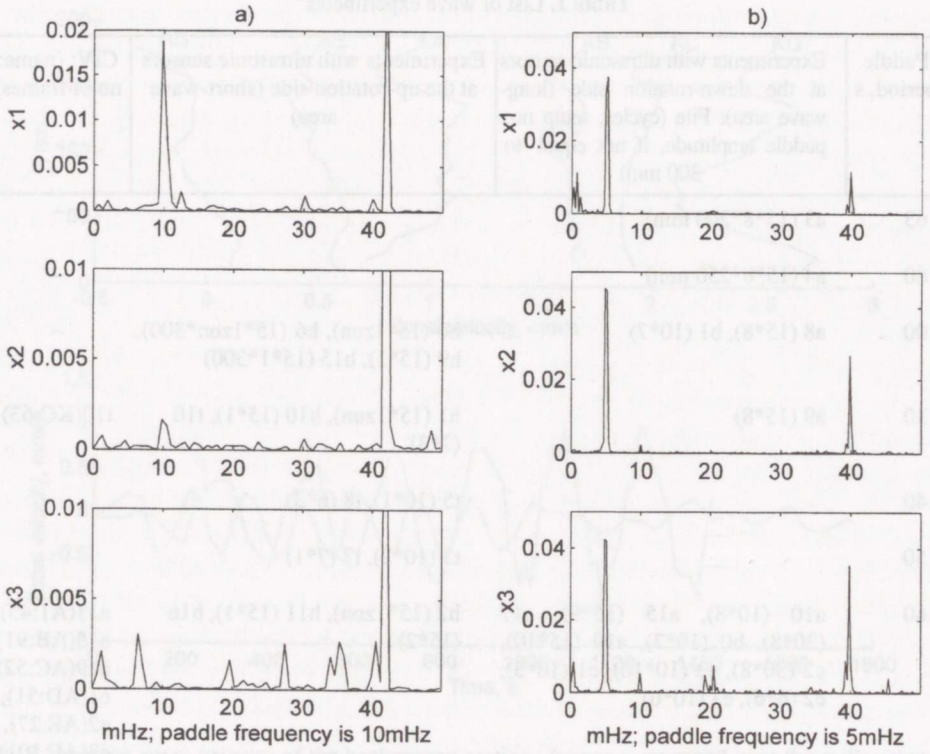

Fig. 4. Power spectra of velocity time series at the contact measurement points. The data are not smoothed, only a few clearly erroneous values have been excluded. Point x1 is the closest to the paddle at the long-wave side. a) $P = 100$ s (experiment a8); b) $P = 200$ s (a18).

lower as compared to the short waves (Fig. 4b). The distinction probably occurs owing to the following reasons. First, the paddle was small as compared to wavelengths of the long-wave side ($\lambda > 10$ m). Second, the longer waves have higher group velocity than the shorter ones, thus, they more effectively transform energy to the absorbing region.

The velocity field in the Mercator co-ordinates, induced by a westward travelling Rossby wave in a zonal channel, consists of a sequence of virtual vortice-like structures (Fig. 5a). In the mixed geometry, they penetrate to some extent beyond the slope (Fig. 5b). The diagrams confirm that wave patterns in the CIV area in the middle of the slope are practically independent of the presence of the barrier. In the actual geometry, the wave trajectories should be piecewise straight (instead of circles for westward travelling waves in radially symmetric basins or straight lines in Mercator co-ordinates), since they may turn somewhat at the bottom segment junctions.

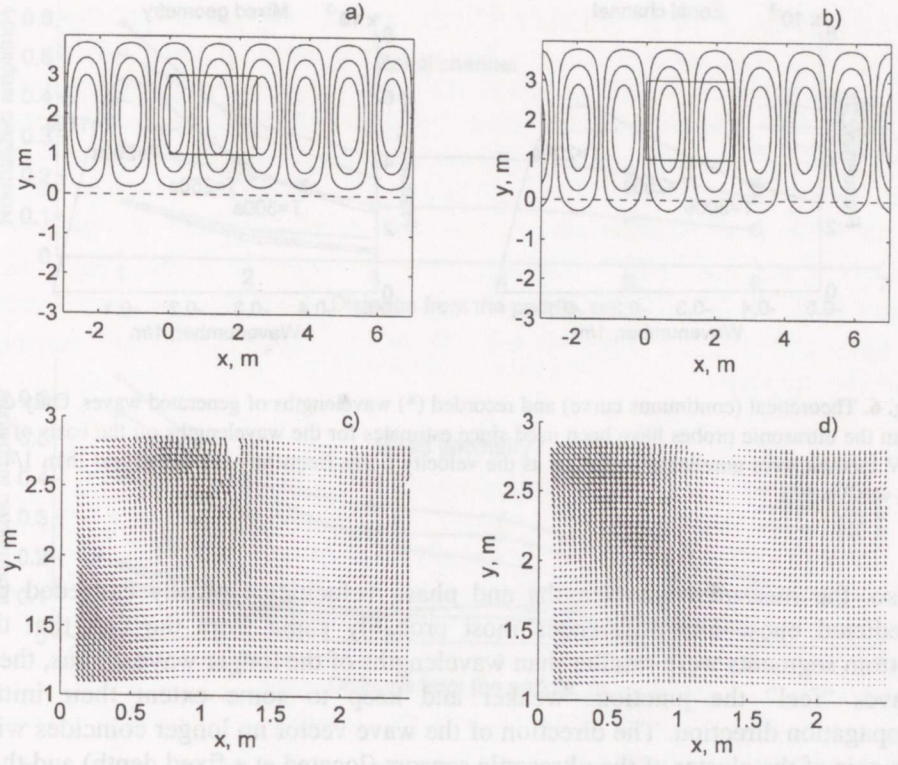

Fig. 5. Theoretical and measured patterns of streamlines of Rossby waves in the Mercator co-ordinates: a), b) streamline patterns for the zonal channel and the mixed geometry, respectively, for $P = 300$ s; c), d) sequential velocity fields for $P = 300$ s at the short-wave side (experiment t9).

Figure 5c shows the velocity field of shorter waves in the experiment with $P = 300$ s. The paddle is located at a distance 2 m eastwards from the measurement area. The diagrams demonstrate the presence of a nearly classical Rossby wave except that its trajectory is modified by the actual bottom geometry. The wave deviates somewhat to the north as it propagates westwards; explanation to this effect is given below.

Note that Kelvin waves, although visible in spectral pictures, are not easily detectable from the 2D velocity fields since they only result in certain stretching or compressing of the whole field. Also, they have been mostly filtered out together with the oscillations with the half-rotation period of the tank owing to the exposure time 5–10 s of the CIV method.

Figure 6 demonstrates that for shorter waves (longer periods) the measured and predicted wavelengths showed a fairly good concordance. For periods $P \approx T_{\min}$ as well as for longer waves a relatively big discrepancy was observed.

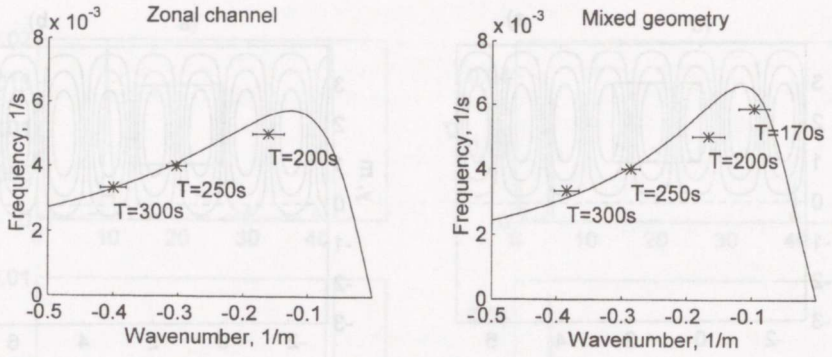

Fig. 6. Theoretical (continuous curve) and recorded (*) wavelengths of generated waves. Only data from the ultrasonic probes have been used since estimates for the wavelengths on the basis of the CIV method were unreliable inasmuch as the velocity fields frequently contained less than 1/4 of the wavelength.

Also, the measured wavelengths and phase velocities typically exceeded the predicted ones. The differences most probably came from the fact that the bottom segments were smaller than wavelengths of the longer waves. Thus, these waves "feel" the junctions weaker and keep to some extent their initial propagation direction. The direction of the wave vector no longer coincides with the axis of the cluster of the ultrasonic sensors (located at a fixed depth) and they record longer "seeming" wavelengths. (Owing to this effect the wave trajectories generally tend to decline to the north.) The form of the dispersion relation also indicates that close to the minimum wave period wave parameters are sensitive to small disturbances of the period.

Amplitude of waves with $P \geq 200$ s diminished nearly twice between the first and the second measurement points but further decreased insignificantly (Fig. 7). Waves with $P = 200$ s were relatively poorly defined in the zonal channel but clearly distinguishable in the mixed geometry. Disturbances with $P < 200$ s had much smaller amplitudes at the closest probe and they decreased faster than other waves. Thus, one may virtually estimate the actual minimum Rossby-wave period in the zonal channel as close to 200 s while for the mixed geometry it is somewhat smaller.

Several results of the spectral analysis of the ultrasonic velocity data suggest another possibility to establish the value $T_{min} \approx 160$ s for the mixed geometry. Namely, in many experiments with $P < 150$ s, in the measurement points remote from the paddle well-defined peaks arose at about 6 mHz (Fig. 4b). This phenomenon may be interpreted as transformation of the generated disturbances into the Rossby wave with the minimum period.

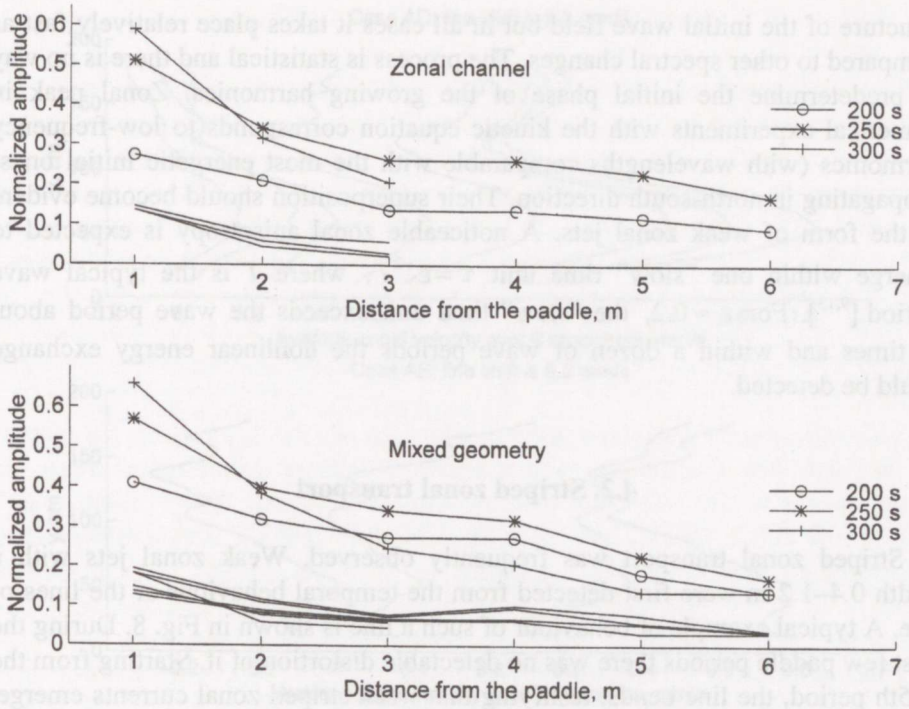

Fig. 7. Amplitudes of oscillations at the frequency of the paddle. Only data concerning the radial velocity component have been used since the paddle frequency was practically absent in the zonal velocity. The amplitudes have been normalized to the paddle amplitude. The non-marked graphs correspond to experiments with $P < 200$ s.

4. NONLINEAR EFFECTS

4.1. Weak nonlinearity and its influence

The velocities of fluid particles were, typically, much less than phase velocities. Their ratio ε (a traditional measure of nonlinearity) is in most cases less than or equal to 0.2. An exception formed the closest vicinity of the paddle in experiments with $P = 250$–300 s and with very small phase velocities. However, starting from the distance 1.5 m from the paddle, the wave amplitudes decreased and this ratio reduced to $\varepsilon \approx 0.2$–0.3. Thus, the restriction of weak nonlinearity was valid for the most of the experimental area except (seldom) in the near-wave field.

Owing to inhomogeneous bottom geometry and the presence of borders, the monochromatic wave field should soon excite a spectrally broad wave field. The latter evolves according to the kinetic theory, in particular, it supports zonal motion components [9,13]. The (nearly) zonal flow generation depends on the

structure of the initial wave field but in all cases it takes place relatively fast as compared to other spectral changes. The process is statistical and there is no way to predetermine the initial phase of the growing harmonics. Zonal peak in numerical experiments with the kinetic equation corresponds to low-frequency harmonics (with wavelengths comparable with the most energetic initial ones) propagating in north-south direction. Their superposition should become evident in the form of weak zonal jets. A noticeable zonal anisotropy is expected to emerge within one "slow" time unit $\tau = \varepsilon^{-2}T$, where T is the typical wave period [9,13]. For $\varepsilon \approx 0.2$, the "slow" time unit exceeds the wave period about 20 times and within a dozen of wave periods the nonlinear energy exchange could be detected.

4.2. Striped zonal transport

Striped zonal transport was frequently observed. Weak zonal jets with a width 0.4–1.2 m were first detected from the temporal behaviour of the lines of dye. A typical example of behaviour of such a line is shown in Fig. 8. During the first few paddle periods there was no detectable distortion of it. Starting from the 4–5th period, the line bends, testifying that weak striped zonal currents emerge. The zonal velocity was about 0.05 mm/s. The translatory velocity of the water was not detectable (less than 0.01 mm/s).

In the long-wave experiments we observed generation of weak striped zonal flow in all experiments with CIV measurements on the basis of the meridional average of 2D velocity fields. Zonal flow in the long-wave side of the paddle always became evident after about 5 paddle periods and continued to grow until the end of the experiments (Fig. 9). Its structure showed a great variability and no two experiments were similar to each other. The width of the stripes varied from 0.3 to 0.9 m (formally corresponding to somewhat shorter waves than the

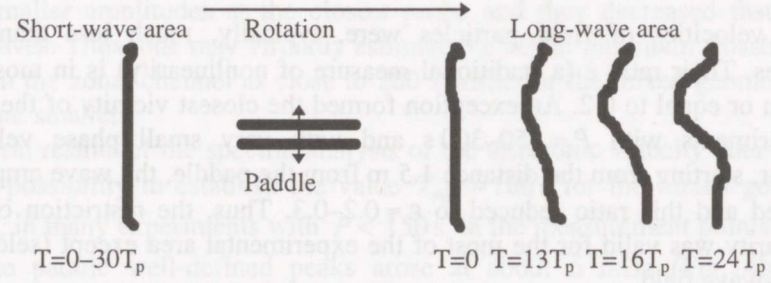

Fig. 8. Temporal evolution of a dye line in experiment with P = 200 s (a18). The line (length about 1.5 m) was located at 2 m from the paddle axis in the middle of the sloping bottom. Its sequential forms are shifted for better readability.

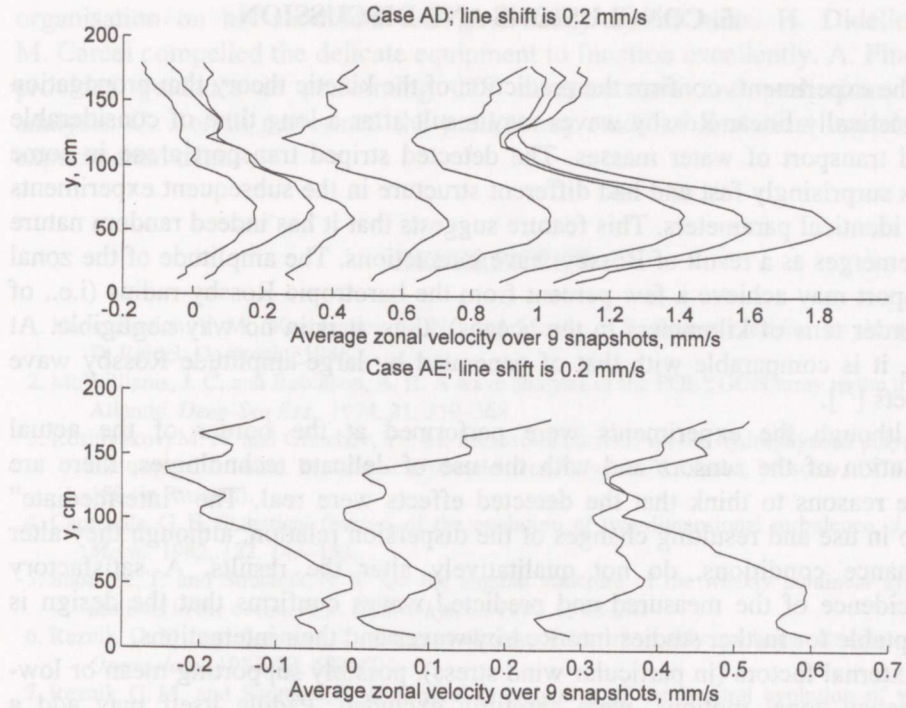

Fig. 9. Temporal evolution of averaged zonal velocity in the CIV measurement area in experiments AD and AE. The graphs represent zonal velocity averaged over several sequential snapshots. For better comparison, the sequential graphs are shifted by 0.2 mm/s.

generated ones). The maximum zonal velocity varied from 0.04 (relatively narrow stripes in experiment AE) to 0.4 mm/s (wide stripes in experiment AD). The average zonal velocity over more than two wave periods never exceeded 0.01 mm/s (cf. Fig. 3). Analysis of sequential experiments shows that the jets persisted, at least, a few dozens of minutes. In some cases they caused zonal transport of water up to the first dozens of centimetres, a distance comparable with the amplitude of the primary waves.

Zonal transport in the short-wave area was much weaker than in the long-wave region. Bending of a dye line was not visually detectable. Analysis of 2D velocity fields shows that in the short-wave area the typical (background) zonal velocity field consisted of weak jets with typical width 0.4–1.0 m. They slowly propagated north- or southwards but were practically not amplified during the experiments. An explanation to this distinction probably consists in the fact that the shorter waves "feel" the bottom inhomogeneities more. They skirt more along the bottom isolines, reflect less from the outer wall and, thus, generate less random wave components.

5. CONCLUSIONS AND DISCUSSION

The experiments confirm the prediction of the kinetic theory that propagation of practically linear Rossby waves may result after a long time of considerable zonal transport of water masses. The detected striped transport arose in some cases surprisingly fast and had different structure in the subsequent experiments with identical parameters. This feature suggests that it has indeed random nature and emerges as a result of Rossby-wave interactions. The amplitude of the zonal transport may achieve a few percent from the barotropic Rossby radius (i.e., of the order tens of kilometers in the oceans), thus, it is in no way negligible. At least, it is comparable with that of generated by large-amplitude Rossby wave packets [32].

Although the experiments were performed at the border of the actual resolution of the sensors and with the use of delicate technologies, there are grave reasons to think that the detected effects were real. The "intermediate" setup in use and resulting changes of the dispersion relation, although they alter resonance conditions, do not qualitatively alter the results. A satisfactory coincidence of the measured and predicted waves confirms that the design is acceptable for further studies into Rossby waves and their interactions.

External factors (in particular wind stress), possibly supporting mean or low-frequency zonal motions, were carefully excluded. Paddle itself may add a certain angular component of flow if its blades or oscillation direction are tilted from the ideal position [26]. However, its influence should be present regularly, at least, in experiments with identical parameters but performed at different days or in different sequence (for example, experiments a15, e1, e3). Analysis of the corresponding fields of zonal velocity shows no correlation; thus, the possible role of the paddle in the mean flow excitation can be neglected.

Nonlinear (turbulent) energy cascade generally supports a global vortex or dipole (westward flow in the centre of the slope and eastward flow near the walls of the zonal channel [24]). Figure 3, on the contrary, confirms the absence of any stable zonal flow in the CIV area in the middle of the slope. Careful analysis of dye translation within somewhat larger area, observed by the analogue video recorder, also confirmed the absence of any regular zonal transport.

ACKNOWLEDGEMENTS

The experiment was financed by the Scientific Commission of the European Community in the framework of the program Human Capital and Mobility – Access to Large Devices (contracts ERBCIPD940092 and ERBCGHECT920015). The final stage of the study was sponsored by the Estonian Science Foundation (grant 3504/98).

The invaluable contribution of the team of the "Coriolis" Laboratory for completing the experiment is gratefully acknowledged. D. Renouard took local

organisation on his shoulders and gave many useful hints. H. Didelle and M. Carcel compelled the delicate equipment to function excellently. A. Fincham provided guidance in performing CIV measurements and preliminary data analysis. C. Borghi performed the preliminary study of analytical models and experimental data.

REFERENCES

1. Kamenkovich, V. M., Koshlyakov, M. N., and Monin, A. S. *Synoptic Eddies in the Ocean.* D. Reidel, Dordrecht, 1986.
2. McWilliams, J. C. and Robinson, A. R. A wave analysis of the POLYGON array in the tropical Atlantic. *Deep-Sea Res.*, 1974, **21**, 359–368.
3. Koshlyakov, M. N. and Gratchev, Yu. M. Mesoscale currents on the hydrophysical polygon in the tropical Atlantic. In *Atlantic Hydrophysical Polygon-70.* Nauka, Moscow, 1974, 163–180 (in Russian).
4. Carnevale, G. F. Statistical features of the evolution of two-dimensional turbulence. *J. Fluid Mech.*, 1982, **122**, 143–153.
5. Soomere, T. and Strachuk, N. K. On the angular structure of the weakly nonlinear synoptic motions in the ocean. *Mar. Hydrophys. J.*, 1990, **6**, 28–34.
6. Reznik, G. M. and Soomere, T. On generalized spectra of weakly nonlinear Rossby waves. *Oceanology*, 1983, **23**, 692–694.
7. Reznik, G. M. and Soomere, T. Numerical investigation of the spectral evolution of weakly nonlinear Rossby waves. *Oceanology*, 1984, **24**, 287–294.
8. Reznik, G. M. and Soomere, T. On the evolution of an ensemble of Rossby waves to an anisotropic equilibrium state. *Oceanology*, 1984, **24**, 424–429.
9. Reznik, G. M. Weak turbulence on a β-plane. In *Synoptic Eddies in the Ocean.* D. Reidel, Dordrecht, 1986, 73–108.
10. Soomere, T. Generalized stationary solutions of the kinetic equation of barotropic Rossby waves. *Oceanology*, 1987, **27**, 407–409.
11. Kozlov, O. V., Reznik, G. M., and Soomere, T. Weak turbulence on the β-plane in a two-layer ocean. *Izv. Acad. Nauk SSSR, Fiz. Atmosfery i Okeana*, 1987, **23**, 869–874 (in Russian).
12. Soomere, T. Generation of zonal flow and meridional anisotropy in two-layer weak geostrophic turbulence. *Phys. Rev. Lett.*, 1995, **75**, 2440–2443.
13. Soomere, T. Spectral evolution of two-layer weak geostrophic turbulence. Part 1. Typical scenarios. *Nonlinear Proc. Geophys.*, 1996, **3**, 166–195.
14. Korotayev, G. K. *Structure, Dynamics and Energetics of Oceanic Synoptic Variability.* Preprint No. 7, Marine Hydrophysical Institute, Sevastopol, 1980 (in Russian).
15. Ekman, V. M. On the influence of the earth's rotation on ocean currents. *Arkiv för Matematik, Astronomi och Fysik*, 1905, **2**.
16. Fultz, D. and Frenzen, P. A note on certain interesting ageostrophic motions in a rotating hemisphere shell. *J. Meteor.*, 1955, **12**, 332–338.
17. Fultz, D. and Kaylor, R. The propagation of frequency in experimental baroclinic waves in a rotating annular ring. In *The Atmosphere and the Sea in Motion* (Bolin, B., ed.). The Rockefeller Institute Press, Oxford University Press, New York, 1959, 359–371.
18. Phillips, N. A. Elementary Rossby waves. *Tellus*, 1965, **17**, 295–301.
19. Ibbetson, A. and Phillips, N. Some laboratory experiments on Rossby waves in a rotating annulus. *Tellus*, 1967, **19**, 81–87.
20. Pedlosky, J. and Greenspan, H. P. A simple laboratory model for the oceanic circulation. *J. Fluid Mech.*, 1967, **27**, 291–304.

21. Holton, J. An experimental study of forced barotropic Rossby waves. *J. Geophys. Fluid Dyn.*, 1971, **2**, 323–337.
22. Beardsley, R. C. The 'sliced-cylinder' laboratory model of the wind-driven ocean circulation. Part 2. Oscillatory forcing and Rossby wave resonance. *J. Fluid Mech.*, 1975, **69**, 41–64.
23. Beardsley, R. C. and Robbins, K. The 'sliced-cylinder' laboratory model of the wind-driven ocean circulation. Part 1. Steady forcing and topographic Rossby wave instability. *J. Fluid Mech.*, 1975, **69**, 27–40.
24. Colin de Verdière, A. *Quasigeostrophic Flow and Turbulence in a Rotating Homogeneous Fluid.* Ph. D. Thesis, Massachusetts Inst. of Technology/Woods Hole Oceanographic Institution, 1977.
25. Whitehead, J. A. Jr. Mean flow generated by circulation on a β-plane: An analogy with the moving flame experiment. *Tellus*, 1975, **27**, 358–364.
26. Faller, A. J. The origin and development of laboratory models and analogues of the ocean circulation. In *Evolution of Physical Oceanography* (Warren, B. A. and Wunsch, C., eds.). MIT Press, Cambridge, Massachusetts, 1981, 462–479.
27. Nezlin, M. V. Rossby solitons. *Adv. Phys.*, 1986, **150**, 3–60.
28. Fincham, A. M. and Spedding, G. R. Low cost, high resolution DPIV for measurement of turbulent fluid flow. *Exp. Fluids*, 1996, **23**, 449–462.
29. Kamenkovich, V. M. and Reznik, G. M. Rossby waves. In *Physics of the Ocean, vol. 1*: *Hydrophysics.* Nauka, Moscow, 1978, 300–358 (in Russian).
30. Gill, A. E. *Atmosphere-Ocean Dynamics.* Academic Press, New York, London, 1968.
31. Borghi, C. *Ondes de Rossby*: *une étude expérimentale.* Ecole Centrale Paris, Université Pierre et Marie Curie, Laboratoire CORIOLIS, Inst. de Méchanique de Grenoble, 1996.
32. Lacasce, J. H. and Speer, K. G. Lagrangian spectra in Rossby wave fields. *Ann. Geophys*, 1997, **15**, Suppl., C561.

LINEAARSED ROSSBY LAINED JA TSONAALNE TRANSPORT PÖÖRLEVAL PLATVORMIL

Tarmo SOOMERE ja Tiit KOPPEL

Pöörleval platvormil "Coriolis" (läbimõõt 13 m) uuriti Rossby laineid ning nende interaktsioone. Geograafiline β-efekt modelleeriti 50-ruutmeetrise kaldpõhja abil. Suhteliselt väikese radiaalsuunas liigutatava laba abil tekitati praktiliselt lineaarsed lained, milles veeosakeste kiirus oli suurusjärgus 1 mm/s. Mitmetes eksperimentides fikseeriti nõrgad tsonaalsed jugahoovused iseloomuliku laiusega 0,4–1,0 m ning kiirusega kuni 0,4 mm/s. Vee ümberpaiknemine nendes ulatus lainegeneraatori amplituudini. Tõenäoliselt indutseeris hoovused stohhastilise Rossby lainete välja komponentide mittelineaarne interaktsioon.